F009

Joint Interpretation of Multiple Passive Seismic Data Volumes

B.W. Artman (Spectraseis AG), A. Goertz* (Spectraseis AG), B. Schechinger (Spectraseis AG), P. Krajewski (GDF SUEZ E&P Deutschland GmbH) & M. Koerbe (GDF SUEZ E&P Deutschland GmbH)

SUMMARY

Geologic interpretation is best realized by joint interpretation of multiple geophysical techniques. After recording a 25 station, 7.5km linear passive array for over 48h, we divide the data into four time subsets characterized by total energy content. We investigate the 4 volumes with methods where the subsets satisfy the assumptions underlying the techniques. The first volume contains high total energy associated with anthropogenic noise. We analyze it with Rayleigh wave ellipticity velocity inversion. The second volume is 45s around a M5.9 teleseismic event. This data is analyzed for site amplification indications. The third subset has low energy content from 01:00 Sunday. This data is analyzed for departures from the background Rayleigh wave solution provided by volume 1. Fourth, 10-180s intervals are selected from the Sunday morning data and depth imaged with time-reversal algorithms. Finally, we interpret the results in an integrated framework. The first two volumes characterize the regional ambient wavefield, and indicates that the shallow subsurface is largely constant across the profile. The second two volumes indicate that there is observable body wave content providing local subsurface information from depth. 1D excess energy anomalies and 2D energy focusing are consistent with each other and an oil reservoir.

Introduction

Forty-eight hours, spanning a weekend, of ambient seismic records were collected in two 7.5 km lines with 25 broadband seismometers through a town of approximately 50,000 residents. The lines were positioned to cross a recently discovered oil reservoir, centered beneath the town. For conciseness, we focus this discussion on only one of the profiles. We subdivide the data into four distinct volumes. The first data set is ~36 hours from the day time intervals of Saturday and Sunday. The raw data is characterized by high energy content. Transients on a given trace are rarely identifiable on more than its two nearest neighbors. The second time window is in contrast only 45 s long around a teleseismic arrival of an M 5.9 earthquake. The third volume is a very low energy time window extracted between 00:00 and 07:00 on Sunday morning. Some short transients are visible and can often be traced several kilometers across the line. Such time intervals were muted to prepare this data set. Last, segments of 10-180 s were selected from the low energy volume three to process with (algorithmically more expensive) time-reversal imaging.

High energy data volume one is analyzed in the framework of ellipticity analysis of fundamental mode Rayleigh waves (Okada, 2003). This method assumes that all energy in a 1D time series can be explained by the Fourier ellipticity ratio as the convolution of continuous excitation and the local near surface velocity structure. This method is commonly used for estimating site amplification analysis for use in earthquake resistant structural engineering. Because of a fortunate teleseismic arrival during a relatively quiet time interval, a second measure of potential site amplification due to local velocity structure is extracted directly. In the early hours of the weekend mornings, anthropogenic noise sources are at a minimum. During this time interval, data set three is mined for body wave content due to subsurface heterogeneities. To do so, we assume that body waves are distinct from surface waves in 1D Fourier analysis by being quasi-linearly polarized with sub-vertical dip as compared to elliptically polarized Rayleigh waves (Aki and Richards, 2002, Saenger et al., 2009). Lastly, short time windows within this data that comprise data set four will be reverse propagated and imaged with the time-reverse imaging (Witten and Artman, 2010) method to focus the subsurface location of the body wave content in the data.

Data 1 – high energy surface waves

The stations in this survey were directly within urban areas and the day-time records are rich in broadband surface wave energy. With no editing in time, stable Fourier ratios of the horizontal over vertical particle velocity are calculated. These curves, H/V(f), are inverted for 1D velocity models assuming the energy in the records is strictly due to the fundamental Rayleigh mode (Panza, 1985, Wathelet, 2008). Initial velocity models were derived from some combination of 3D seismic velocities, statics estimation, and refraction tomography. The individually inverted velocity profiles all conform to a reasonable distribution of plausible depth functions beginning with surface P velocities around 500 m/s with 3 or 4 layers to 100 m depth achieving approximately 2000 m/s. The deeper profiles all return stable gradients of ~1 km/s/km in the sedimentary section down to basement, at approximately 3.5 km.

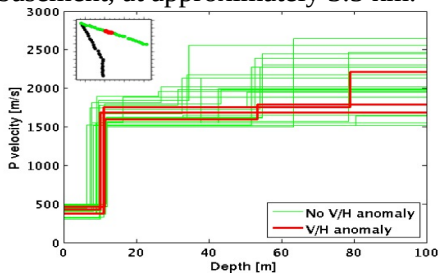

Figure 1 *Velocity profiles inverted from Rayleigh ellipticity. Colors show spatial distribution of 1D models along the line. Red curves labeled V/H anomaly explained in Data 3 section.*

Beginning the inversions with fairly good velocity control from other experiments gives confidence in the results despite the fact that some features in the H/V spectral ratios were not well explained by the assumption that the data contain only fundamental mode Rayleigh waves. However, the main conclusion from the analysis is that the family of results is stable across the line. No families of stations grouped together along the line occupy distinctly different segments of the distribution of results, and the results are not bi-modal. Specifically, the velocity model inversions cannot explain the grouping of stations highlighted in red in Figure 1 that follows from the analysis below of data volume three.

Data 2 – teleseismic earthquake arrival

At approximately 23:25 (local) Sunday morning, body waves from a M5.9 earthquake from the mid-Atlantic ridge arrived at the receiver line. There is no move-out of the arrival across the 7.5 km array. The data were band-passed from 0.2-2.0 Hz and the peak amplitude of the P and S–wave arrivals were picked and compared. Immediately before the arrival, the amplitude of the 0.2 Hz microseism were picked in the frequency domain. Plotting these profiles along the acquisition line shows that energy from the two different frequency bands generally follow the same pattern across the line. Also, the central part of the line, indicated between dashed lines, does not show distinctly different character than the rest of the stations.

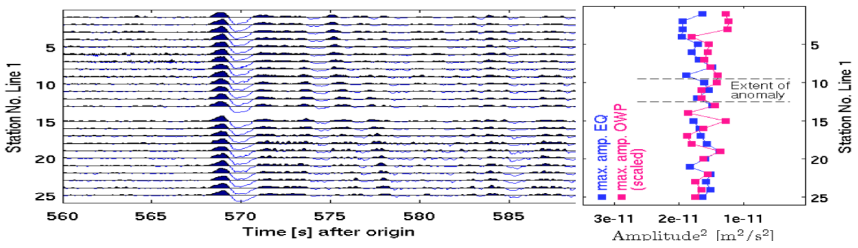

Figure 2 *Teleseismic M 5.9 earthquake arrival and amplitude extraction (blue). Amplitude of the ocean microseism evaluated in the frequency domain (red) multiplied by 50.*

Data 3 – low energy body wave Fourier domain analysis

In the very early hours of Sunday morning, data records have characteristically low energy content with occasional transient events that are removed before further analysis. Under the assumption that the ambient wave field is composed of both surface wave energy and body waves due to subsurface scattering, we process the data to focus on energy content that is not characteristic of surface waves. Because Rayleigh wave hodograms, over a half-space, are characterized by vertical over horizontal particle motion of approximately 0.8, the addition of linearly polarized P-waves from below to a linear system will increase the ratio above the background level. Having already inverted the high energy data volume one for a subsurface velocity model, we also have available the forward modeled Rayleigh wave ellipticity curves that best fit the observed data. Departures from the modeled curves that have higher V/H values are measured as a proxy for linearly polarized energy that we assume is due to body wave arrivals.

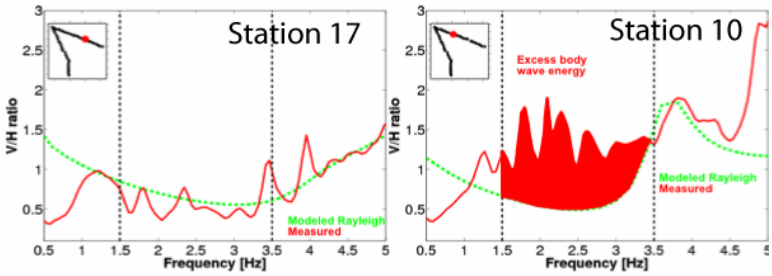

Figure 3 *V/H(f) functions for two stations calculated with night data (solid) and forward modeled Rayleigh wave solutions calculated with noisy data (dashed). Red area (right) is attribute calculation used to plot profiles.*

Figure 3 shows V/H spectra from two stations from the array with location included in the subset. The forward modeled Rayleigh wave is the dashed line. The solid line is the spectral ratio from the low energy data. Both stations show good agreement outside of the interval between the vertical lines. Station 10, however, shows a major departure. This indicates that the Rayleigh wave assumption is only partially correct for station 10. These data contain both surface waves and anomalous energy characterized by particle velocity ratios larger than background. Additional P-wave energy from below explains such observations. We acknowledge that such analysis is not a true decomposition of the two signal modes. The red integrated area in the right panel is calculated as a measure of the body wave content in the data, though it does contain surface wave contamination.

The same analysis and integral attribute calculation (red area, Figure 3) was performed across the profile for 40s time windows of 7 hours of the edited, quietest night-time data. Figure 4 shows the mean and standard deviation of the attribute as a function of time window (Riahi et. al, 2009). The

vertical axis has been normalized by the bandwidth of the integral. Arrows point to stations in Figure 3. The vertical dashed lines in the center of the profile group the stations that all contain extra body wave energy over background. This group of central stations, with this low energy data set, cannot be explained by the Rayleigh wave assumption. This same group was indicated in Figures 1 and 2, but did not stand out from the others when analyzing the other two, high energy, volumes of data.

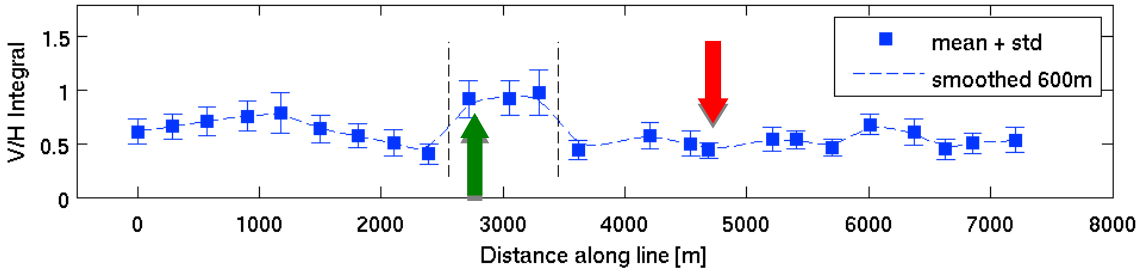

Figure 4 *Body wave energy in the quiet night data as measured by the amount of anomalous linearly polarized energy by integrating V/H(f) as in Figure 3. Green arrow points to station 10, red to 17.*

Data 4 – low energy body wave time domain analysis

An interval velocity model for the region was produced from a previous 3D seismic survey. Short duration (seconds to minutes) data from the low energy night records were used for time-domain reverse modeling (Fink, 1999) studies. In addition to reverse-time propagation, we add mode decomposition, time axis collapse via correlation, and signal-to-noise (S/N) estimation in the resulting image domain (Witten and Artman, 2010). The total algorithm is called time-reverse imaging (TRI). The TRI method locates in depth subsurface sources and/or scattering events that give rise to body waves in the data. We imaged 5 time windows of 3 m duration as well as many 30-10 s time windows within those 15 min to produce estimated S/N images from the P-, S-, and PS-wave potential wave fields (Artman, 2009). High S/N values within these images indicate potential source/scattering locations. However, due to the variable nature of the ambient wave field, and inaccuracies of the noise model used to estimate the S/N images, we prefer to process as much data in time as computationally feasible and look for stable focusing in the many results. Subsurface content should remain stable, while artifacts should be randomly distributed in time and space.

Figure 5 shows a P-wave S/N image and a similar result with forward modeled data (right) made with a single force at the location of the white dot. Both show strong signal w.r.t. background level in the center of the image. This energy focus is laterally shifted ~1.5 km to the right (down dip) of the surface V/H anomaly shown in Figure 4.

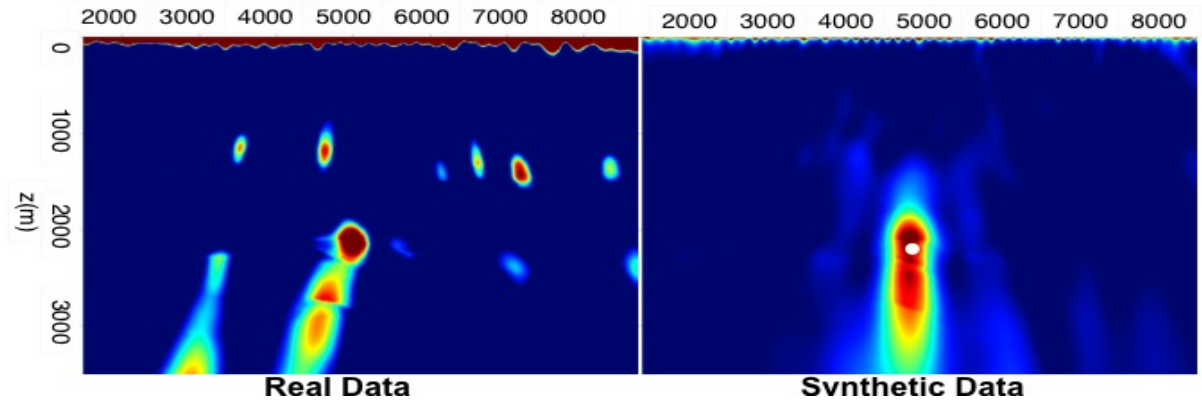

Figure 5 *Three minutes of field data compared to a synthetic time-reverse imaging result to locate the subsurface source of body waves within passive data.*

Synthesis

Four different data sets were analyzed to investigate the information content of the ambient wave field at this site. The first volume contained predominantly high-energy Rayleigh waves with little local

variation along the profile. The earthquake data set also leads to the conclusion that significant local amplification of the wave field along the profile is not expected or measured. The other two data volumes from very quiet time intervals are in fact overlapping, where the amount of data analyzed in the time domain is limited only due to computation expense. We assume however that during this interval, significant processes within the ambient wave field are sufficiently stable that the information content in the data volumes is comparable. In both cases, body wave content carrying information from the subsurface is evident and largely collocated in their shared (surface) spatial dimension. We assume that the energy located with the different techniques is the same. Further, there is no correlation between the distribution of body wave energy extracted from the low energy data sets with the profiles generated from the high energy (day time and earthquake) data sets.

Conclusion

The earth structure along the line of this transect of recordings is roughly layer-type geology down to a thrusting fault-block at the basement depth. The background ambient wave field during lengthy intervals is stable in this region and consistent along the line. This allows velocity measurements with surface wave assumptions when source wave field requirements are met (Aki, 1956). The results of such efforts allow calculation of the forward modeled site response of every station. Departures from this background model are then used to investigate body wave content in different time intervals. During the low energy night-time time intervals, the data are not explainable by only Rayleigh waves. Instead, the anomalous energy in the surface ellipticity ratio, calculated in the Fourier domain, and subsurface focusing of body wave energy performed with time-reverse imaging collocate anomalous energy in the low energy data volume.

At several kilometers depth under the center of the receiver line there is a producing oil reservoir under the four central stations along the profile. The synthesis of the four analysis techniques leads us to the conclusion that the reservoir is the only viable local inhomogeneity that is acting as a weak secondary scatterer that adds body wave content to the ambient wave field. During active times of high anthropogenic energy, this weak signal is masked by Rayleigh waves with rich azimuthal distribution. During the quiet time interval however, body wave energy can be associated at depth and laterally with the reservoir as mapped by 3D seismic and wells.

References

Aki, K. [1957] A note on the use of microseisms in determining the shallow structures of the Earth's crust, Geophysics, **30**, 665-666.

Aki, K. and Richards, P. [2002] Quantitative Seismology, 2nd ed., University Science Books.

Artman, B., Podladtchikov, I., and Goertz, A.[2009] Elastic time-reverse modeling imaging conditions, SEG Technical program expanded abstracts, **28**, 1207.

Okada, H. (translated by Suto, K.) [2003] The microtremor survey method, Geophysical monograph series, SEG.

Fink, M. [1999] Time-reversed acoustics: Scientific American, November, 67–73.

Panza, G. F. [1985] Synthetic seismograms: the Rayleigh waves modal summation: J. Geophys., **58**, 125 – 145.

Riahi, N., Kelly, M., Ruiz, M., and Yang, W.[2009] Bayesian DHI using passive seismic low frequency data, SEG Technical program expanded abstracts, **28**, 1607-1611.

Saenger, E. H., Schmalholz, S. M, Lambert, M.-A., Nguyen, T. T., Torres, A., Metzger, S.M., Habiger, R.M., Miller, T., Rentsch, S., and Mendez-Hernandez, E.[2009] A passive seismic survey over a gas field: Analysis of low-frequency anomalies: Geophysics, **74**, O29–O40.

Wathelet, M.[2008] An improved neighborhood algorithm: parameter conditions and dynamic scaling.: Geophysical Research Letters, **35**, L09301.

Witten, B. and Artman, B.[2010] Signal to noise estimates of time-reversal images, 72st EAGE Conference and exhibition, Extended Abstracts, submitted.